Bio-optical characteristics of the western Arctic Ocean: implications for ocean color algorithms

Article *in* Canadian Journal of Remote Sensing · January 2007

CITATIONS
35

READS
72

5 authors, including:

Atsushi Matsuoka
Laval University
32 PUBLICATIONS **1,210** CITATIONS
SEE PROFILE

Yannick Huot
Université de Sherbrooke
58 PUBLICATIONS **1,910** CITATIONS
SEE PROFILE

Koji Shimada
Tokyo University of Marine Science and Technology
80 PUBLICATIONS **2,888** CITATIONS
SEE PROFILE

Sei-Ichi Saitoh
Hokkaido University
202 PUBLICATIONS **3,229** CITATIONS
SEE PROFILE

Can. J. Remote Sensing, Vol. 33, No. 6, pp. 503–518, 2007

Bio-optical characteristics of the western Arctic Ocean: implications for ocean color algorithms

Atsushi Matsuoka, Yannick Huot, Koji Shimada, Sei-Ichi Saitoh, and Marcel Babin

Abstract. Global ocean color algorithms designed to estimate chlorophyll *a* concentration (chl*a*) are not accurate at high latitudes. Although a regional Arctic OC4L algorithm was designed to be applicable to high northern latitudes, its applicability remains uncertain. To examine these issues, we investigated the light absorption coefficients of phytoplankton, non-algal particles (NAP), and colored dissolved organic matter (CDOM) and remote sensing reflectance, $R_{rs}(\lambda)$, covering most of the western Arctic Ocean. A higher pigment packaging effect was identified relative to that at lower latitudes. The CDOM absorption dominated and accounted for 76% of the total non-water absorption at 443 nm and did not covary with variations in chl*a*. This absorption is significantly higher than those in other marine environments. We also examined the backscattering coefficient of particles obtained from the inversion of $R_{rs}(\lambda)$ and found that it covaried well with variation in NAP absorption. Our evaluation shows that when turbid waters ($R_{rs}(670) > 0.00042$ sr^{-1}) are excluded, the performance of the OC4L is good and much better than that of the sea-viewing wide field-of-view sensor (SeaWiFS) OC4V4 and the moderate-resolution imaging spectroradiometer (MODIS) OC3M (root mean square error (RMSE) of 0.13, 0.21, and 0.22, respectively). The reason why the OC4L performs well despite strong CDOM absorption is discussed.

Résumé. Les algorithmes de couleur de l'océan conçus pour l'estimation de la concentration de chlorophylle *a* (chl*a*) ne sont pas précis dans les hautes latitudes. Bien que l'algorithme OC4L régional arctique ait été conçu pour application dans les hautes latitudes nordiques, son applicabilité demeure également problématique. Afin d'examiner ces questions, nous avons analysé le coefficient d'absorption de la lumière du phytoplancton, des particules non algales (NAP), de la matière organique dissoute colorée (CDOM) et la réflectance $R_{rs}(\lambda)$ obtenue par télédétection de la majeure partie de l'ouest de l'Océan arctique. Il a été possible d'identifier un effet de regroupement de pigmentation plus élevé par rapport à celui observé dans les latitudes plus basses. L'absorption de CDOM dominait et comptait pour 76 % du total de l'absorption non liée à l'eau à 443 nm, et ne covariait pas avec la valeur de chl*a*. Ce phénomène est significativement plus élevé que pour les autres environnements marins. Nous avons également étudié le coefficient de rétrodiffusion des particules obtenu par l'inversion de $R_{rs}(\lambda)$ et nous avons observé qu'il covariait bien avec l'absorption de NAP. Notre évaluation indique que, lorsque les eaux turbides ($R_{rs}(670) > 0.00042$ sr^{-1}) sont exclues, la performance de l'algorithme OC4L est bonne et bien meilleure que celle de OC4V4 de SeaWiFS (« sea-viewing wide field-of-view sensor ») et OC3M de MODIS (« the moderate-resolution imaging spectroradiometer ») (RMSE (« root mean square error ») = 0,13, 0,21 et 0,22, respectivement). Nous discutons des raisons pour lesquelles l'algorithme OC4L performe bien en dépit de la forte absorption de CDOM.
[Traduit par la Rédaction]

Introduction

High primary production (PP) has been reported in the western Arctic Ocean (up to 860 g C·m^{-2}·year^{-1}) (Springer et al., 1996; Chen et al., 2002). This high PP suggests that the western Arctic Ocean is not a biological desert as previously thought but has an active carbon cycle. Although the continuous measurement of PP is essential to accurately estimate its impact on the global carbon cycle, field campaigns are necessarily restricted both geographically and temporally by sea ice cover. Satellite remote sensing using ocean color sensors in polar regions may fill the gap.

In addition to irradiance, the most important parameter to estimate PP using remote sensing is the chlorophyll *a* concentration (chl*a*). In polar regions, however, a series of studies has reported that chl*a* estimated by global ocean color

Received 15 August 2007. Accepted 26 November 2007. Published on the *Canadian Journal of Remote Sensing* Web site at http://pubs.nrc-cnrc.gc.ca/cjrs on 8 February 2008.

A. Matsuoka[1] and S.-I. Saitoh. Laboratory of Marine Bioresource and Environment Sensing, Graduate School of Fisheries Sciences, Hokkaido University, 3-1-1 Minato-cho, Hakodate, Hokkaido, 041-8611, Japan.

Y. Huot and M. Babin. Laboratoire d'Océanographie de Villefranche, Centre National de la Recherche Scientifique, Université Pierre et Marie Curie (Paris 6), 06238, Villefranche-sur-Mer Cedex, France.

K. Shimada. Japan Agency for Marine-Earth Science and Technology, 2-15 Natsushima-cho, Yokosuka, Kanagawa, 237-0061, Japan.

[1]Corresponding author (atsushi@salmon.fish.hokudai.ac.jp).

algorithms was significantly different from in situ chl*a* (Mitchell and Holm-Hansen, 1991; Mitchell, 1992; Arrigo et al., 1998; Dierssen and Smith, 2000; Sathyendranath et al., 2001; Cota et al., 2003; Stramska et al., 2003; Wang and Cota., 2003; Cota et al., 2004; Wang et al., 2005). There are two main causes for this discrepancy.

First, bio-optical properties in polar waters are significantly different from those in waters at lower latitudes (Mitchell and Holm-Hansen, 1991; Mitchell, 1992; Arrigo et al., 1998; Sathyendranath et al., 2001; Cota et al., 2003; Stramska et al., 2003; Wang et al., 2005). The difference was mainly attributed to the presence of large-size phytoplankton such as diatoms, which leads to highly packaged phytoplankton absorption. This leads to an underestimation of chl*a* by global algorithms roughly by a factor of 1.5 in the Labrador Sea (Cota et al., 2003). Cota et al. (2003) additionally mentioned that the high contribution of the absorption coefficient of colored dissolved organic matter (CDOM), $a_{CDOM}(\lambda)$, to the total non-water absorption, $a_{t\text{-}w}(\lambda)$, may have a significant impact on chl*a* estimates by ocean color algorithms. This conclusion supports previous studies and emphasizes the importance of CDOM absorption at high northern latitudes (Carder et al., 1989; Sathyendranath et al., 2001). This is consistent with the fact that the Arctic Ocean is the basin that receives the largest amount of freshwater relative to its volume (11% of global freshwater input while its volume is 1% of the Global Ocean; Shiklomanov, 1993). However, the lack of measurements of CDOM absorption (e.g., Mitchell, 1992; Stramska et al., 2003) has prevented us from characterizing the light absorption behavior by each component directly, namely, phytoplankton, non-algal particles (NAP), and CDOM. More recently, in our study region, the western Arctic Ocean (**Figure 1**), Wang et al. (2005) described the trends of these absorption coefficients, namely, the absorption coefficient of phytoplankton ($a_{\varphi}(\lambda)$), the absorption coefficient of NAP ($a_{NAP}(\lambda)$), and the absorption coefficient of CDOM ($a_{CDOM}(\lambda)$), as a function of chl*a* and compared their results with those at lower latitudes. However, this study leaves the following important questions unanswered: (*i*) Which constituent (phytoplankton, NAP, or CDOM) dominates the light absorption of these waters? (*ii*) Which constituents can have a significant impact on chl*a* estimates by ocean color algorithm?

The second cause for the failure of ocean color algorithms lies in the fact that a small number of data points from polar regions was used to develop global ocean color algorithms (e.g., O'Reilly et al., 2000). More recently, Cota et al. (2004) developed an Arctic OC4L ocean color algorithm using a large dataset (number of data points $N = 686$) from data obtained at high northern latitudes (but not exclusively in the Arctic Ocean). This algorithm is designed to be applicable to high northern latitudes, where chl*a* by SeaWiFS ocean chlorophyll four-band version 4 (OC4V4) is underestimated by a factor of 2 over most of the natural range of biomass chl*a* > 0.6 mg·m^{-3} (Cota et al., 2004). This bias is, however, different in the western Arctic Ocean, where chl*a* tends to be overestimated by OC4V4 across the range 0.07–9.00 mg·m^{-3} (Wang and Cota,

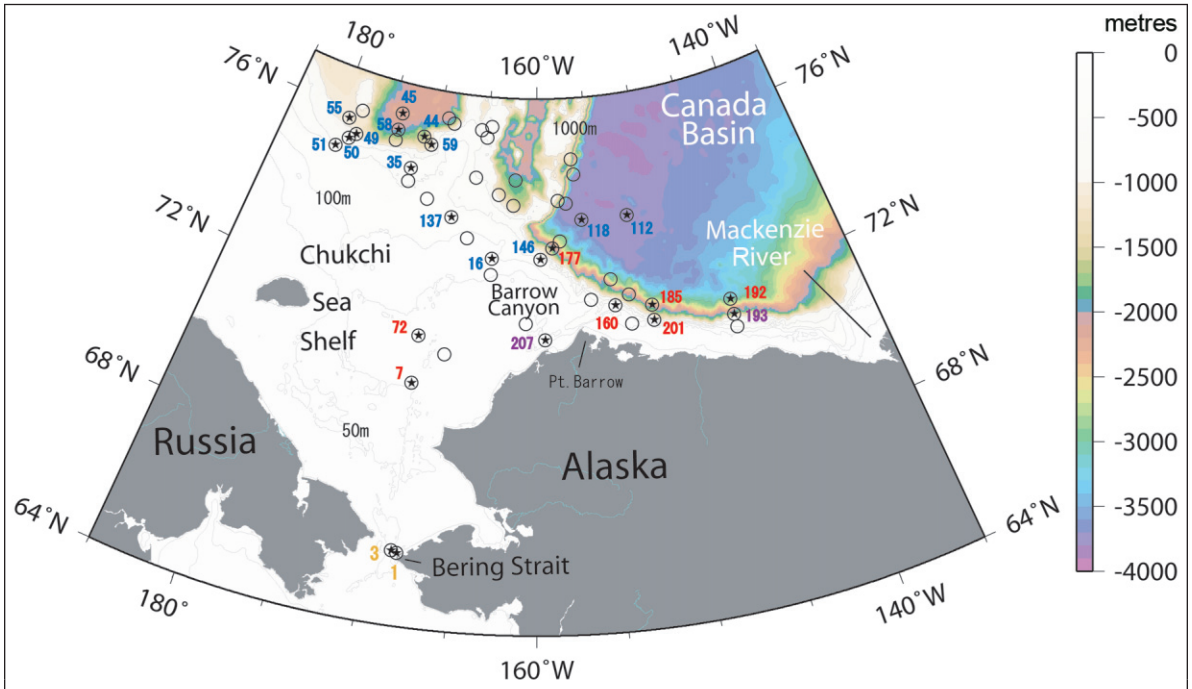

Figure 1. Locations and station numbers for the MR04-05 cruise in the western Arctic Ocean. Circles represent stations where water was sampled, and stars represent stations where radiometric measurements were conducted. Colors are used to identify the station classified in different spectral groups according to their $R_{rs}(\lambda)$ spectra: group A (red), group B (purple), group C (yellow), and group D (blue). See the section titled Evaluation of ocean color algorithms and **Figure 8** for details.

2003). Since ratios of remote sensing reflectance used by the aforementioned two algorithms are related to the absorption and backscattering coefficients (see the next section for details), this discrepancy indirectly implies that the optical properties of the western Arctic Ocean show different relationships with chl*a* than the relationship obtained by Cota et al. (2004) that used a large dataset from various environments at high northern latitudes. However, these properties have not been adequately documented, and the Arctic OC4L has not yet been evaluated.

Thus, the objectives of this study are to (*i*) describe statistically the bio-optical characteristics of the western Arctic Ocean; and (*ii*) evaluate the accuracy of the Arctic OC4L and OC4V4 algorithms, which are often applied to the Arctic Ocean. We also evaluate the OC3M algorithm, which is the operational algorithm for the moderate-resolution imaging spectroradiometer (MODIS) ocean color sensor.

To achieve these objectives, we first describe the characteristics of $a_\varphi(\lambda)$, $a_{NAP}(\lambda)$, and $a_{CDOM}(\lambda)$ versus chl*a*, including their magnitudes and proportions compared with the total non-water absorption. With these absorption coefficients, we also examine the properties of the backscattering coefficient of particles. The spectral shapes of remote sensing reflectance and its relation to hydrographic features are discussed in the next section. Based on these analyses, we reevaluate the accuracy of the Arctic OC4L, the OC4V4, and OC3M algorithms and explain the reasons for their varying accuracy in the western Arctic Ocean.

Background: relationship between inherent optical properties (IOPs) and apparent optical properties (AOPs)

In addition to the structure of incident light field and observation geometry, two inherent optical properties (IOPs) determine the quantity and quality of the light leaving the ocean. The first property is the total absorption coefficient of seawater, $a_t(\lambda)$ (in m^{-1}), where λ is the wavelength dependence (see the List of symbols), which represents the total light absorption due to various constituents in natural waters including water molecules. It can be expressed as the sum of the absorption coefficient of all particles, $a_p(\lambda)$, $a_{CDOM}(\lambda)$, and pure seawater, $a_w(\lambda)$:

$$a_t(\lambda) = a_p(\lambda) + a_{CDOM}(\lambda) + a_w(\lambda) \quad (1)$$

where $a_p(\lambda)$ can be further divided into the contributions of $a_\varphi(\lambda)$ and $a_{NAP}(\lambda)$:

$$a_p(\lambda) = a_\varphi(\lambda) + a_{NAP}(\lambda) \quad (2)$$

The second property is the total backscattering coefficient ($b_b(\lambda)$, in m^{-1}), another IOP, which can be expressed as follows:

$$b_b(\lambda) = b_{bp}(\lambda) + b_{bw}(\lambda) \quad (3)$$

where $b_{bp}(\lambda)$ and $b_{bw}(\lambda)$ are the backscattering coefficients of particles and water molecules, respectively; $b_b(\lambda)$ determines the amount of light backscattered toward the atmosphere within the ocean surface layer and is thus important to applications of ocean color remote sensing (e.g., Stramski et al., 2004).

In open ocean waters, both the absorption and backscattering coefficients covary with variations in chl*a* (e.g., Morel and Maritorena, 2001). Furthermore, two apparent optical properties (AOPs), the remote sensing reflectance ($R_{rs}(\lambda)$, in sr^{-1}) and the normalized water-leaving radiance ($L_{wn}(\lambda)$, in $\mu W \cdot cm^{-2} \cdot nm^{-1} \cdot sr^{-1}$), which are quantities measured by satellite ocean color sensors, can be expressed in terms of these IOPs:

$$R_{rs}(\lambda) = 0.544\left[\frac{f}{Q}\right]\left[\frac{b_b(\lambda)}{a_t(\lambda) + b_b(\lambda)}\right] \quad (4a)$$

$$L_{wn}(\lambda) = F_0 R_{rs}(\lambda) \quad (4b)$$

where 0.544 is a factor describing the effect of the water–air interface; f and Q are empirical factors and are a function of the solar zenith angle θ_s, λ, and chl*a* (Morel et al., 2002); and F_0 is the solar extraterrestrial irradiance. These relationships form the basis of present ocean color algorithms to determine chl*a* and other accessory pigments (e.g., O'Reilly et al., 1998; 2000; Esaias et al., 1998; Carder et al., 1999).

In this study, we evaluate the accuracy of three ocean color algorithms that are often applied to the Arctic Ocean, namely the Arctic OC4L developed by Cota et al. (2004), SeaWiFS OC4V4 (O'Reilly et al., 1998; 2000), and MODIS OC3M (O'Reilly et al., 2000). These algorithms are expressed as follows:

$$\text{chl(OC4L)} = 10^{(a+bR)}$$
$$R = \log(R_{rs}(443 > 490 > 510 / 555)) \quad (5a)$$
$$a = 0.592,\ b = -3.607$$

$$\text{chl(OC4V4)} = 10^{(a_1 + b_1 R + c_1 R^2 + d_1 R^3 + e_1 R^4)}$$
$$R = \log(R_{rs}(443 > 490 > 510 / 555)) \quad (5b)$$
$$a_1 = 0.366,\ b_1 = -3.067,\ c_1 = 1.930,\ d_1 = 0.649,\ e_1 = -1.532$$

$$\text{chl(OC3M)} = 10^{(a_2 + b_2 R' + c_2 R'^2 + d_2 R'^3 + e_2 R'^4)}$$
$$R' = \log(R_{rs}(443 > 488 / 551)) \quad (5c)$$
$$a_2 = 0.2830, b_2 = -2.753, c_2 = 1.457, d_2 = 0.659, e_2 = -1.403$$

where R is the base 10 logarithm of the maximum band ratio (MBR), whichever is the greatest of $R_{rs}(443)/R_{rs}(555)$, $R_{rs}(490)/R_{rs}(555)$, and $R_{rs}(510)/R_{rs}(555)$; R' is the same as R but is for the greater of the two band ratios $R_{rs}(443)/R_{rs}(551)$ and $R_{rs}(488)/R_{rs}(551)$; and the coefficients a, b, a_1, b_1, c_1, d_1, e_1, a_2, b_2, c_2, d_2, and e_2 are empirically derived values.

Methodology

Field observations were made on board the Japanese vessel R/V *Mirai* from 1 September to 12 October 2004 in the western Arctic Ocean (referred to as mission MR04-05) spanning approximately the area from latitudes 65° to 76°N and longitudes 145° to 180°W (**Figure 1**). Temperature and salinity profiles were obtained at 250 stations using a SeaBird 911 conductivity–temperature–depth (CTD) probe coupled with a transmissometer (WET Labs, Inc.).

Water samples for chl*a* and absorption measurements were collected using Niskin bottles, except at the surface where a polyethylene container was used. In total, 183 water samples were collected at 51 stations. Radiometric measurements were also conducted at 25 of these stations following the SeaWiFS protocols (Muller and Austin, 1995). We generally encountered calm seas (averaged wind speed was 6.0 $m \cdot s^{-1}$) and mostly cloud-covered conditions with some sunny periods. Chl*a* was determined fluorometrically with dimethylformamide (DMF) using a 10-AU field fluorometer (Turner Designs) (Holm-Hansen et al., 1965; Suzuki and Ishimaru, 1990). Excluding station 207 where the water was highly turbid (for details, see the section titled Evaluation of ocean color algorithms), the measured chl*a* was strongly correlated with the in situ fluorescence (determination coefficient $r^2 = 0.90$, $N = 141$) measured by the fluorometer (Seapoint Sensors, Inc.) attached to the CTD probe. Based on this relationship, we calculated chl*a* at a 1 m interval using the in situ fluorescence data. These data were then used to obtain the average chl*a* within the surface layer above the first optical depth, z_{90} (in m), which corresponds to the layer from which approximately 90% of the upwelling radiance detected by remote sensors originates (Gordon and McCluney, 1975) (for the calculation, see the section titled Apparent optical properties (AOPs)).

Inherent optical properties (IOPs)

Discrete water samples were collected for absorption measurements over the euphotic zone, z_e (in m; 1% of surface light level), the depth of which reached up to 70 m in this study region. All suspended particles including phytoplankton and NAP were filtered under low vacuum on Whatman GF/F glass fiber filters. We first measured optical density (OD) (Kirk, 1994) of all suspended particles, $OD_p(\lambda)$, from 400 to 750 nm with 1 nm intervals using a MPS2400 spectrophotometer (Shimazu Corp.). Phytoplankton pigments were then extracted with methanol (Kishino et al., 1985), and the OD of the NAP, $OD_{NAP}(\lambda)$, was determined in the same way as that for $OD_p(\lambda)$. Then, $a_\varphi(\lambda)$ and $a_{NAP}(\lambda)$ were calculated (Mitchell, 1990; Cleveland and Weidemann, 1993) using 750 nm for both baselines. The regression analysis as a power function was conducted for all $a_\varphi(\lambda)$ versus chl*a* from 400 to 700 nm. The chl*a*-specific absorption coefficient of phytoplankton, $a_\varphi^*(\lambda)$ (in $m^2 \cdot mg\ chl a^{-1}$), was determined by dividing $a_\varphi(\lambda)$ by chl*a*. The modeled spectra of $a_\varphi^*(\lambda)$ at chl*a* concentrations of 0.1, 0.5, and 1.0 $mg \cdot m^{-3}$ were obtained using the fitted relationships of $a_\varphi(\lambda)$ versus chl*a* divided by chl*a* from 400 to 700 nm with 5 nm intervals above z_{90}. The OD of CDOM, $OD_{CDOM}(\lambda)$, was measured from 400 to 700 nm with 1 nm intervals using the MPS2400 spectrophotometer (Shimazu Corp.) after water samples were filtered on a 0.22 µm Millipore membrane. The $a_{CDOM}(\lambda)$ was calculated from $OD_{CDOM}(\lambda)$ according to the SeaWiFS protocols (Muller and Austin, 1995). The $a_t(\lambda)$ was obtained by summing $a_\varphi(\lambda)$, $a_{NAP}(\lambda)$, and $a_{CDOM}(\lambda)$, with the value of $a_w(\lambda)$ from Pope and Fry (1997) (Equations (1) and (2)).

Wang and Cota (2003) showed that the performance of the model of Lee et al. (2002) when used to estimate $b_{bp}(\lambda)$ from the reflectance spectrum, which was built for open ocean and coastal water environments at temperate latitudes, was quite accurate in the Beaufort and Chukchi seas. In this study, we also employed this model to examine the properties of $b_{bp}(\lambda)$. Briefly, $b_{bp}(\lambda)$ was computed after the Lee et al. model was run with our measured $a_t(\lambda)$ and $R_{rs}(\lambda)$ (see later in the paper). The value of $b_b(\lambda)$ was then obtained as the sum of $b_{bp}(\lambda)$ and $b_{bw}(\lambda)$ (Equation (3)). The values for $b_{bw}(\lambda)$ were taken from Morel (1974). The accuracy of the computed value of $b_{bp}(\lambda)$ is discussed later in the paper (see the section titled Properties of backscattering coefficient of particles).

Apparent optical properties (AOPs)

Profiles of downwelling irradiances, $E_d(\lambda, z)$ (in $\mu W \cdot cm^{-2} \cdot nm^{-1}$), and upwelling radiances, $L_u(\lambda, z)$ (in $\mu W \cdot cm^{-2} \cdot nm^{-1} \cdot sr^{-1}$), were obtained using an in-water PRR-600 spectroradiometer (Biopherical Instruments, Inc.) with a PRR-610 reference deck unit. Both units had centre wavelengths of 412, 443, 490, 520, 565, and 670 nm. The PRR-600 included a tilt sensor, and the measurements were made to minimize ship shadow from the back deck away from the ship body. The tilt angles were always within ±10°, as recommended by the SeaWiFS protocols (Muller and Austin, 1995), except for those of two stations (7 and 137), where they reached 11° or 13° during downwelling measurements with the PRR-600. Since $R_{rs}(\lambda)$ calculated from these spectra did not depart from the other values (see **Figure 8**), we decided to keep these two stations for our analysis. The value of $L_u(\lambda, z)$ just below the sea surface, $L_u(\lambda, 0^-)$, was obtained by extrapolation of the logarithm-transformed data from 1–3 m (Darecki and Stramski, 2004). The value of $L_u(\lambda, 0^-)$ was then multiplied by 0.544 to calculate the water-leaving radiance just above the sea surface, $L_w(\lambda, 0^+)$ (Darecki and Stramski, 2004). The value of $E_d(\lambda, 0^+)$ measured using the PRR-610 deck unit was averaged during the same time periods as the $L_u(\lambda, z)$ measurements from 1–3 m, and lastly the value of $R_{rs}(\lambda, 0^+)$ was obtained using $E_d(\lambda, 0^+)$ and $L_w(\lambda, 0^+)$:

$$R_{rs}(\lambda, 0^+) = \frac{L_w(\lambda, 0^+)}{E_d(\lambda, 0^+)} = 0.544 \frac{L_u(\lambda, 0^-)}{E_d(\lambda, 0^-)} \quad (6)$$

To apply the Arctic OC4L, OC4V4, and OC3M algorithms, $R_{rs}(488)$, $R_{rs}(510)$, $R_{rs}(551)$, and $R_{rs}(555)$ are required but were not measured at those exact wavelengths. Dierssen and Smith

(2000) pointed out that the interpolation scheme developed by O'Reilly et al. (1998; 2000) might not be appropriate in polar regions where bio-optical properties are different from those at lower latitudes. Therefore, we conducted simple linear interpolation to obtain $R_{rs}(\lambda)$ at the right wavelengths using the measured values. The $R_{rs}(\lambda)$ spectra including these interpolated $R_{rs}(\lambda)$ values are similar to those obtained by Wang and Cota (2003) in the same study region (see the section titled Evaluation of ocean color algorithms).

The value of z_{90} was calculated following two different methods in this study: (*i*) if radiometric data were available for a given station, the diffuse attenuation coefficient of downwelling irradiance ($K_d(490)$; in m^{-1}) was calculated from $E_d(490, z)$ measurements from 1–3 m based on a least squares regression technique, and z_{90} was calculated as $1/K_d(490)$; (*ii*) if no radiometric data were available for a given station, $K_d(490)$ was calculated from the measured $a_t(\lambda)$, modeled $b_b(\lambda)$, and θ_s according to Lee et al. (2005). Because no $R_{rs}(\lambda)$ data were available, $b_b(\lambda)$ (a small contribution to $K_d(490)$) was estimated from the significant relationship between $b_b(\lambda)$ and $a_t(\lambda)$ (**Table 1**). The value of z_{90} was then determined as $1/K_d(490)$.

Results and discussion

Characteristics of light absorption coefficients of phytoplankton, NAP, and CDOM

We first investigate the general trends of the light absorption coefficients of phytoplankton, NAP, and CDOM in the western Arctic Ocean and compare them with those in other world ocean basins. A power function is applied to examine the relationship between the absorption coefficients for each component and chl*a*, assuming that the function is appropriate to represent these relationships (Bricaud et al., 1995; 1998). In view of the application of ocean color algorithms, all samples are divided into two layers, one above z_{90} and one below z_{90}. We describe the bio-optical characteristics for each layer separately.

We found a high correlation between the absorption coefficient by the total particulate fractions and chl*a* (phytoplankton plus NAP) as well as for phytoplankton only ($r^2 = 0.75$ and 0.80, respectively, for all samples in **Table 2** and **Figure 2**). The strength of these correlations is comparable to those from previous results for other environments (i.e.,

Table 1. Determination coefficients (r^2; N = 25) between modeled $b_b(\lambda)$ and measured $a_t(\lambda)$ at 412, 443, 490, 510, and 555 nm used for ocean color algorithms.

Wavelength (nm)	r^2
412	0.92
443	0.94
490	0.95
510	0.95
555	0.89

Note: The wavelengths correspond to the bands of the SeaWiFS.

Table 2. Coefficients for power laws expressed as $a_x(\lambda) = A_x(\lambda)[\text{chl}a]^{E_x(\lambda)}$ at 443 nm for each component.

	A_p	E_p	r^2(p)	A_φ	E_φ	$r^2(\varphi)$	A_{NAP}	E_{NAP}	r^2(NAP)	A_{CDOM}	E_{CDOM}	r^2(CDOM)	A_t	E_t	r^2(t)	N
This study ($<z_{90}$)	0.0422	0.783	0.82	0.0304	0.887	0.80	0.0109	0.594	0.54	0.0913	0.350	0.35	0.1438	0.421	0.60	94
This study ($>z_{90}$)	0.0414	0.588	0.73	0.0283	0.784	0.80	0.0109	0.326	0.27	0.0892	0.063	0.05	0.1476	0.199	0.40	89
This study (all)	0.0403	0.659	0.75	0.0288	0.820	0.80	0.0104	0.424	0.35	0.0858	0.167	0.14	0.1401	0.281	0.43	183
Bricaud et al. (1998)	0.0520	0.635	0.91	0.0378	0.627	0.90	0.0124	0.724	0.73	—	—	—	—	—	—	1166
Cota et al. (2003)	0.0542	0.544	0.80	0.0402	0.578	0.73	0.0151	0.410	0.55	0.0502	0.086	0.02	—	—	—	—*
Wang et al. (2005)	0.0511	0.585	0.79	0.0151	0.957	0.89	0.0306	0.296	0.41	0.0509	0.197	0.18	—	—	—	157

Note: The subscript x represents either the total particulate fractions (p), phytoplankton (φ), non-algal particles (NAP), CDOM, or total components including the fraction of pure seawater (t); λ is the wavelength (which is not repeated in the table for brevity). Available coefficients in the literature are also shown for comparison.

*The number of samples is different for each component as follows: N = 257 for $a_p(443)$; N = 175 for $a_\varphi(443)$; N = 175 for $a_{NAP}(443)$; N = 159 for $a_{CDOM}(443)$.

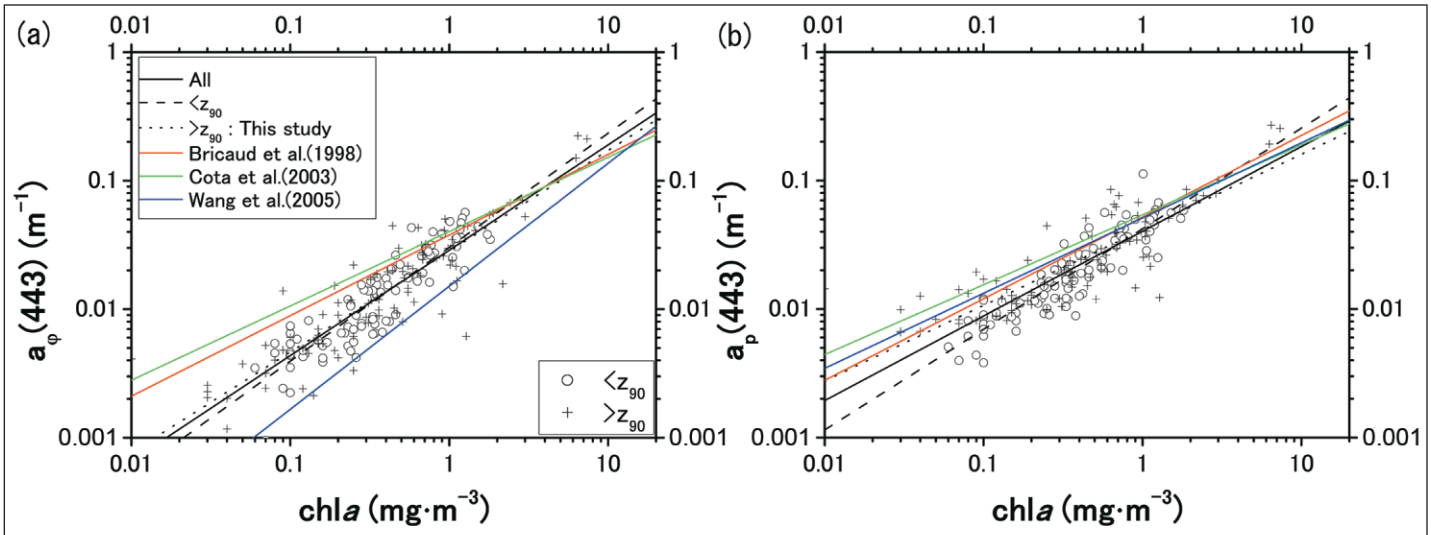

Figure 2. Relationships between absorption coefficients for (a) phytoplankton and (b) the total particulate fractions (phytoplankton plus NAP) and chl*a*. Data are separated according to whether samples are above (open circles) or below (crosses) one optical depth (z_{90}). Regression curves are shown for each set and for the two sets together. Results from the literature are also shown for comparison (i.e., Bricaud et al., 1998; Cota et al., 2003; Wang et al., 2005). These statistics are shown in **Table 2**.

Table 3. Parameters for power laws regression expressed as $a_\varphi(\lambda) = A_\varphi(\lambda)[\text{chl}a]^{E_\varphi(\lambda)}$ from 400 to 700 nm with 5 nm increments.

λ (nm)	*A*	*B*	r^2
400	0.0209	0.881	0.701
405	0.0232	0.898	0.779
410	0.0252	0.902	0.797
415	0.0266	0.891	0.798
420	0.0275	0.881	0.805
425	0.0281	0.878	0.803
430	0.0291	0.866	0.799
435	0.0304	0.863	0.795
440	0.0306	0.860	0.796
445	0.0291	0.857	0.797
450	0.0271	0.856	0.797
455	0.0257	0.855	0.798
460	0.0253	0.858	0.799
465	0.0249	0.854	0.792
470	0.0242	0.854	0.787
475	0.0228	0.847	0.775
480	0.0241	0.843	0.772
485	0.0202	0.845	0.776
490	0.0189	0.853	0.789
495	0.0172	0.858	0.798
500	0.0156	0.866	0.807
505	0.0141	0.874	0.817
510	0.0126	0.877	0.817
515	0.0113	0.877	0.819
520	0.0103	0.888	0.818
525	0.0093	0.894	0.822
530	0.0085	0.909	0.824
535	0.0077	0.924	0.820
540	0.0070	0.950	0.833
545	0.0064	0.965	0.831
550	0.0057	0.975	0.824
555	0.0049	0.970	0.820
560	0.0043	0.972	0.795
565	0.0039	0.947	0.778
570	0.0036	0.932	0.771
575	0.0036	0.946	0.802
580	0.0035	0.894	0.770
585	0.0036	0.904	0.789
590	0.0037	0.903	0.797
595	0.0036	0.890	0.790
600	0.0034	0.880	0.777
605	0.0033	0.867	0.774
610	0.0035	0.891	0.806
615	0.0038	0.895	0.800
620	0.0041	0.912	0.821
625	0.0042	0.907	0.823
630	0.0045	0.909	0.837
635	0.0048	0.898	0.831
640	0.0050	0.898	0.831
645	0.0052	0.870	0.808
650	0.0054	0.883	0.810
655	0.0058	0.903	0.846
660	0.0072	0.920	0.863
665	0.0100	0.930	0.866
670	0.0127	0.922	0.852
675	0.0140	0.921	0.840
680	0.0128	0.932	0.838
685	0.0093	0.951	0.856
690	0.0054	0.956	0.869
695	0.0029	0.969	0.867
700	0.0018	0.993	0.833

Table 3 (*concluded*).

Note: The symbol φ is not repeated in the table for brevity.

Bricaud et al., 1998; Cota et al., 2003; Wang et al., 2005) (see **Table 2** for details). The trends of $a_\varphi(443)$ versus chl*a* from Bricaud et al. (1998) and Cota et al. (2003) are similar but depart strongly from those of both this study and the study of Wang et al. (2005), especially at chl*a* < 2.0 mg·m^{-3} (**Figure 2a**). For chl*a* determination, high-performance liquid chromatography (HPLC) data were adopted by Bricaud et al., but data using the fluorometric method were used for this study and those of Cota et al. and Wang et al. Although large biases are sometimes observed between these two methods (e.g., Marrari et al., 2006), we assume here that this error is not sufficiently large (i.e., less than an factor of 2) to bias the comparison with other methods. Comparing the studies of Cota et al., Wang et al., and Bricaud et al. and our study, we indeed find that the methods do not seem to be at the origin of the differences observed (i.e., the studies of Cota et al. and Bricaud et al. are similar and used fluorometric and HPLC chl*a*, respectively). Here, two possible causes are put forward to explain the observed difference: a pigment packaging effect and (or) pigment composition (e.g., Morel and Bricaud, 1981; Bricaud et al., 1995), resulting from either photoacclimation status or species composition.

Figure 3 shows spectra of $a_\varphi^*(\lambda)$ obtained from the regression analysis of $a_\varphi(\lambda)$ versus chl*a* (see **Table 3**) divided by chl*a* at three chl*a* concentrations of 0.1, 0.5, and 1.0 mg·m^{-3} in addition to the measured spectra. Our results clearly show that our modeled $a_\varphi^*(\lambda)$ is lower than that obtained by Bricaud et al. (1995) for all of the visible spectral domain (but the relative difference is lower in the green bands) for all chl*a* concentrations shown in **Figure 3**. This indicates that the different pigment packaging and (or) changing pigment composition prevails in our study region compared with those at lower latitudes (the two effects are often intermingled and are difficult to separate using our dataset alone) (Bricaud et al., 1995). This result is consistent with previous results at higher latitudes (e.g., Cota et al., 2003; Wang and Cota, 2003; Wang et al., 2005). Although a clear and systematic difference of $a_\varphi(443)$ versus chl*a* between our study and that of Wang et al. (2005) is identified, we cannot examine this difference further because a detailed study of the phytoplankton community was not conducted during our cruise.

The trend of $a_p(443)$ versus chl*a* (**Figure 2b**) shows that the relative locations of the fits are the same as those in **Figure 2a** except for that of Wang et al. (2005), which is relatively close to those of Bricaud et al. (1998) and Cota et al. (2003) with its high A_p value (**Table 2**). Since the total particulate fractions can be divided into phytoplankton and NAP (Equation (2)), this is attributed to a remarkably high A_{NAP} (= 0.0306) from Wang et al. (**Table 2**).

The fraction of $a_p(443)$ due to $a_{NAP}(443)$ is highly variable at chl*a* < 2.0 mg·m^{-3} (**Figure 4a**). This high variability is consistent with previous reports from all latitudes (Bricaud et al., 1998; Cota et al., 2003; Wang et al., 2005), suggesting that this might be a reality in the world oceans. Despite this high variability in all datasets, $a_p(443)$ is mainly due to phytoplankton absorption, with $a_{NAP}(443)$ contributing generally for less than a half of $a_p(443)$ (**Figure 4b**). There is no difference between the two layers.

Figure 5 illustrates the relative proportion of $a_\varphi(\lambda)$, $a_{NAP}(\lambda)$, and $a_{CDOM}(\lambda)$ to the total non-water absorption, $a_{t\text{-}w}(\lambda)$, where five wavelengths were selected corresponding to the bands of the SeaWiFS ocean color sensors. This allows us to examine the variability in the bands that can be used for the ocean color algorithms applied to the Arctic Ocean (see the section titled Evaluation of ocean color algorithms). The 412 nm band is particularly useful for examining the contribution of CDOM

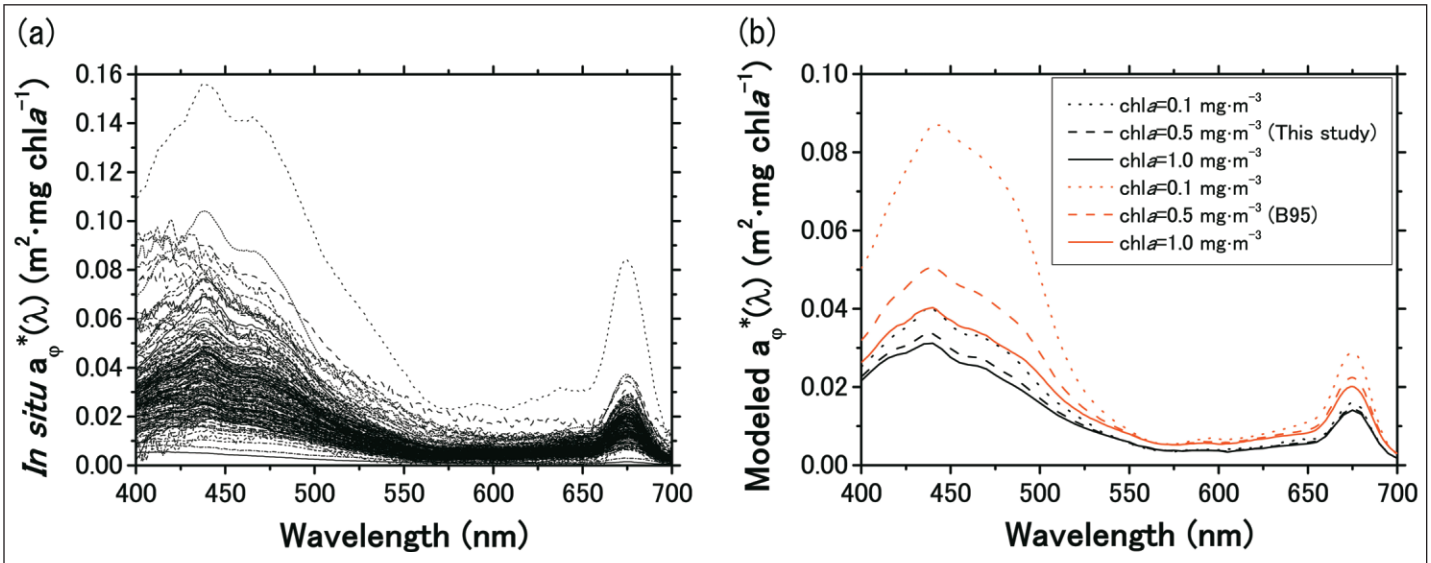

Figure 3. (a) In situ measured spectra of $a_\varphi^*(\lambda)$. (b) Modeled spectra of $a_\varphi^*(\lambda)$ obtained from the fitted relationships of $a_\varphi(\lambda)$ versus chl*a* (see **Table 3**) divided by chl*a* from 400 to 700 nm at chl*a* of 0.1, 0.5, and 1.0 mg·m^{-3}. The spectra at lower latitudes obtained by Bricaud et al. (1995) are shown for comparison (B95).

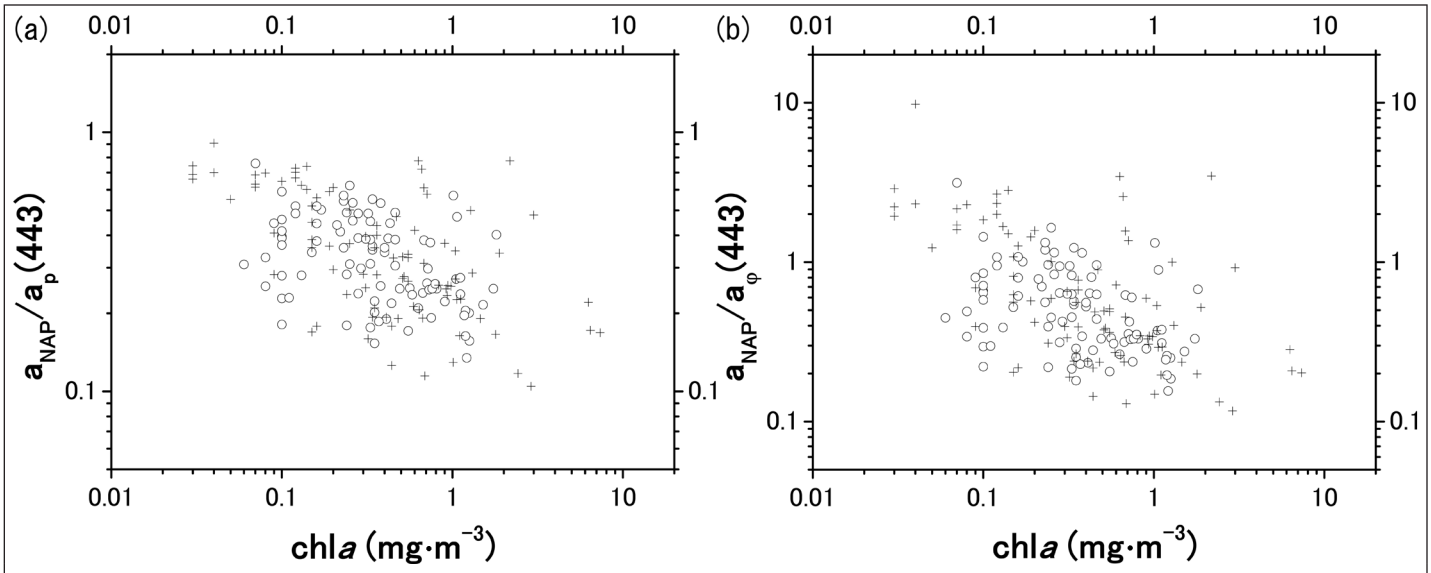

Figure 4. The ratios of (a) $a_{NAP}(443)$ to $a_p(443)$ and (b) $a_{NAP}(443)$ to $a_\varphi(443)$ as a function of chl*a*. Symbols as in **Figure 2**.

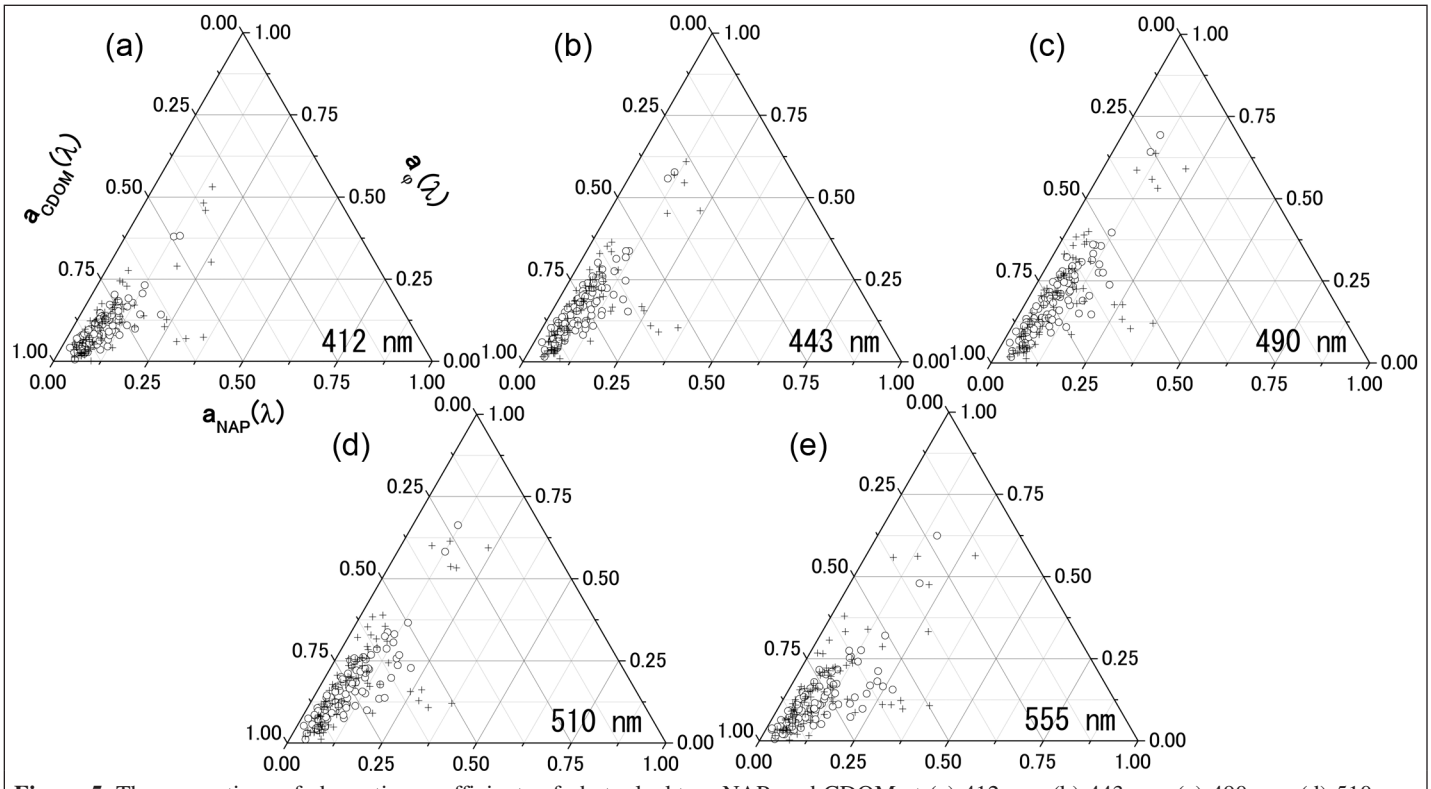

Figure 5. The proportions of absorption coefficients of phytoplankton, NAP, and CDOM at (a) 412 nm, (b) 443 nm, (c) 490 nm, (d) 510 nm, and (e) 555 nm. The wavelengths correspond to the bands of the SeaWiFS. Symbols as in **Figure 2**.

absorption. The optical properties of pure water itself do not influence the classification.

A quick glance at the graphs in **Figure 5** shows that the total non-water absorption coefficient is mainly determined by CDOM. Phytoplankton is the second in importance, and NAP tends to contribute the least. Except for some data points, the proportion of $a_{CDOM}(\lambda)$ to $a_{t\text{-}w}(\lambda)$ is high, contributing to over 50% of $a_{t\text{-}w}(\lambda)$ at all wavelengths, and is particularly high at 412 nm. Even at 443 nm, where phytoplankton absorption is maximal, the contribution of $a_\varphi(\lambda)$ to $a_{t\text{-}w}(\lambda)$ (16%) or the sum of $a_\varphi(\lambda)$ and $a_{NAP}(\lambda)$ to $a_{t\text{-}w}(\lambda)$ are small (24%). On the other hand, the contribution of CDOM in this study is remarkably high at 443 nm (76%) and does not depend on the optical layers (**Table 4**). Our results also show that the fraction of absorption

Table 4. Relative contributions (mean ± 1 SD) of absorption coefficient for phytoplankton (φ), CDOM, and non-algal particles (NAP) to the total non-water absorption $a_{t\text{-}w}(\lambda)$ at 443 nm.

Cruise	Area	Layer	$a_\varphi(443)/a_{t\text{-}w}(443)$	$a_{CDOM}(443)/a_{t\text{-}w}(443)$	$a_{NAP}(443)/a_{t\text{-}w}(443)$	N
This study	Western Arctic Ocean	$<z_{90}$	0.16±0.09	0.76±0.11	0.08±0.03	94
	Western Arctic Ocean	$>z_{90}$	0.16±0.13	0.76±0.15	0.08±0.06	89
	Western Arctic Ocean	All	0.16±0.11	0.76±0.13	0.08±0.05	183
Babin et al. (2003)	Coastal waters around Europe	Surface	0.36±0.14	0.41±0.14	0.22±0.13	317

Note: The values in Babin et al. (2003) are also included for comparison.

by CDOM is significantly higher (0.76 ± 0.13 for all samples) than that measured by Babin et al. (2003) (0.41 ± 0.14), which described the general trend of light absorption coefficients of phytoplankton, NAP, and CDOM in coastal waters around Europe (**Table 4**). This means that CDOM dominates the total light absorption of waters in the western Arctic Ocean, which is in contrast with the findings from studies in other environments (Bricaud et al., 1998; Babin et al., 2003). Similar trends of a high contribution by CDOM absorption are also found from 490 to 555 nm in our data. The fact that CDOM absorption does not covary with variation in chl*a* (r^2 = 0.14 for all samples; **Table 2**) is consistent with previous results at higher latitudes (r^2 = 0.02 in Cota et al., 2003; r^2 = 0.18 in Wang et al., 2005) (see **Table 2**), indicating that current models for CDOM covarying with chl*a* in case 1 waters do not work at higher latitudes. In summary, all of our results suggest that the bio-optical properties in the western Arctic Ocean are different from those in other world oceans. Most importantly, they are strongly influenced by CDOM absorption, and phytoplankton absorption tends to be lower for a given chl*a*, probably due to the packaging effect.

Properties of backscattering coefficient of particles

The backscattering coefficient of particles was computed to evaluate its impact on the reflectance measured by satellite ocean color sensors. **Figure 6a** shows that the magnitude of the computed $b_{bp}(555)$ covers a wide range and is similar to that reported by Wang et al. (2005) ($0.0004 < b_{bp}(555) < 0.013$), who measured it using a HydroScat-6 backscattering meter (HOBI Labs). A relatively low determination coefficient between $b_{bp}(555)$ and chl*a* was found (r^2 = 0.31, N = 24). To give confidence to our estimates and verify that the Lee et al. (2002) model was accurate in this study region, we tested that another product of Lee et al., $a_t(\lambda)$, correlated well with our measured $a_t(\lambda)$ at 412, 443, 490, 510, and 555 nm (**Figure 6b**). Because the accuracy of estimated $b_{bp}(\lambda)$ by the Lee et al. model depends on an accurate determination of $a_t(\lambda)$ and $R_{rs}(\lambda)$ (Lee et al., 2002), validating $a_t(\lambda)$ suggests that the computation of $b_{bp}(\lambda)$ can be trusted. Moreover, this result also suggests that, using the Lee et al. algorithm if $a_{CDOM}(\lambda)$ and $a_{NAP}(\lambda)$ are parameterized appropriately with their spectral slopes (**Table 5**), $a_\varphi(\lambda)$ can be retrieved with relatively good accuracy (or in the opposite case, $a_{NAP}(\lambda)$ and $a_{CDOM}(\lambda)$ can be estimated when $a_\varphi(\lambda)$ is parameterized). In our environment, the quasi-analytical algorithm (QAA) of Lee et al. may thus have potential to retrieve all optical components (i.e., $a_\varphi(\lambda)$, $a_{NAP}(\lambda)$, and $a_{CDOM}(\lambda)$) using ocean color remote sensing.

Although the contribution of $a_{NAP}(\lambda)$ to $a_{t\text{-}w}(\lambda)$ is the lowest, $a_{NAP}(443)$ is highly correlated with $b_{bp}(555)$ (r^2 = 0.85, N = 24, $P < 0.0001$; **Figure 6c**). The value of $a_{CDOM}(\lambda)$ shows a lower correlation with $b_{bp}(555)$ (r^2 = 0.60, N = 24). The correlation between $a_\varphi(\lambda)$ and $b_{bp}(555)$ is the lowest (r^2 = 0.40, N = 24). The strengths of these correlations thus do not depend on the relative contributions by each component (namely, phytoplankton, NAP, and CDOM). Although CDOM is defined as colored *dissolved* organic matter contained in seawater that passes through a 0.22 μm Millipore membrane, the CDOM includes mixed organic–inorganic matter and various types of particles (Stramski et al., 2004). Therefore, the high correlation between $a_{CDOM}(\lambda)$ and $b_{bp}(555)$ found in this study might reflect backscattering by particles smaller than 0.22 μm in size, as mentioned by Wang and Cota (2003). Nonetheless, our results suggest that NAP is the main cause of the backscattering in our study region.

We found that $b_{bp}(555)$ covaries well with variation in $a_{NAP}(443)$ in our environment (**Figure 6c**). Babin et al. (2003) suggested that $a_{NAP}(443)$ was highly correlated with the concentration of suspended particulate matter (r^2 = 0.80, N = 387). Combined, these results suggest that $b_{bp}(555)$ can be modeled as a function of $a_{NAP}(443)$ or SPM. Because in our study the retrieval of $b_{bp}(\lambda)$ requires the knowledge of $a_t(\lambda)$ that includes $a_{NAP}(443)$, $b_{bp}(\lambda)$ is not a completely independent variable (see the section titled Inherent optical properties (IOPs)). However, since the contribution of $a_{NAP}(\lambda)$ to $a_t(\lambda)$ is small (see the previous section for details), its effect on the inversion is also likely to be very small. Since there are far fewer measurements of $b_{bp}(\lambda)$ compared with the absorption measurements, this relationship is useful because it can be used to estimate $b_{bp}(\lambda)$ using the absorption coefficient of NAP.

Evaluation of ocean color algorithms

We tested the performance of the Arctic OC4L algorithm designed to be applicable to high northern latitudes and the global ocean color algorithms, OC4V4 and OC3M, which are often applied to the Arctic Ocean (**Figure 7**). Surface chl*a* used here for our evaluation were highly correlated with the average chl*a* within the water column above z_{90} (r^2 = 0.75, N = 23), which suggests that the average vertical variability of chl*a* is well represented by surface chl*a*, even if the vertical structure is not available. Overall, when considering all sampled stations,

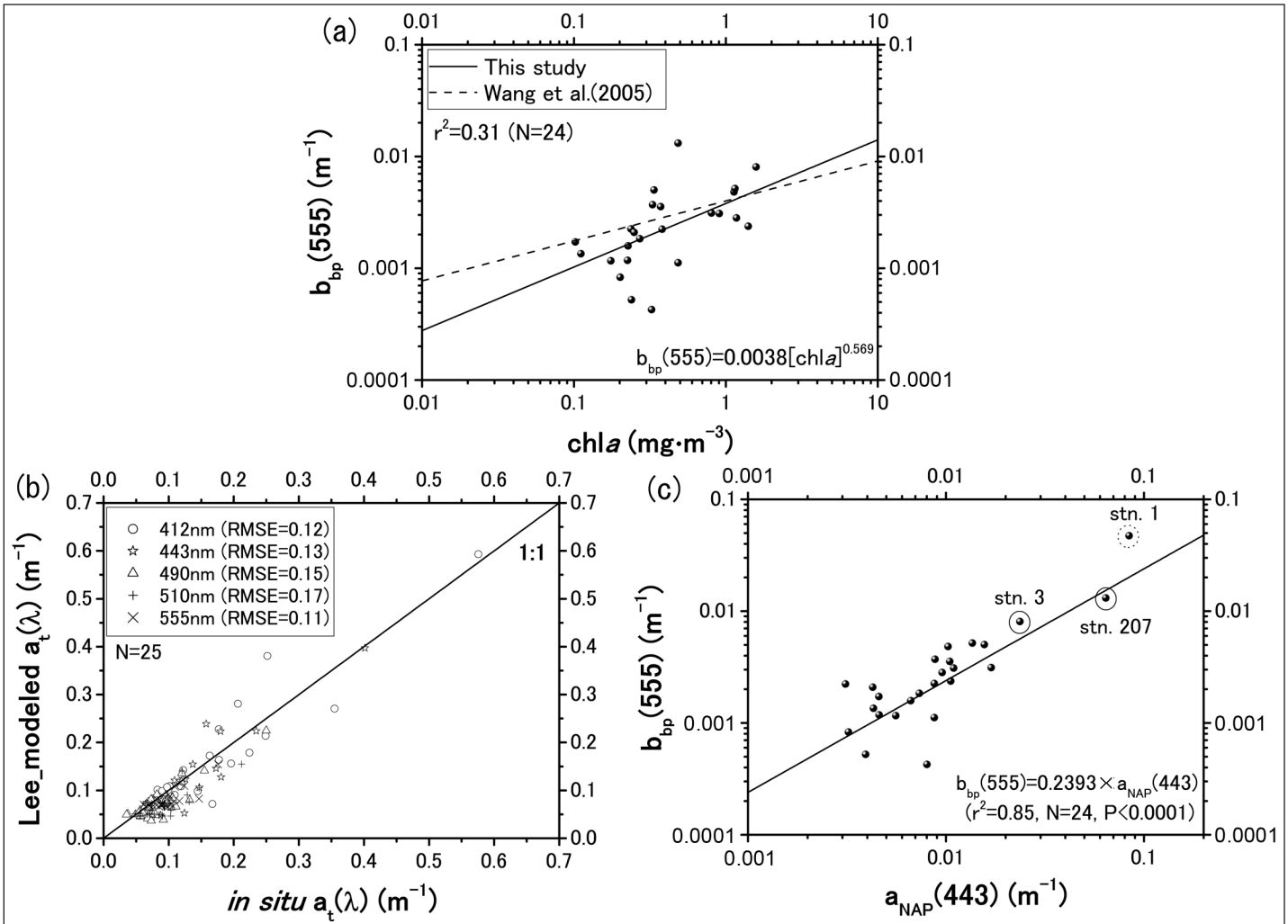

Figure 6. Examination of the backscattering coefficient of particles obtained according to Lee et al. (2002). (a) Relationship between $b_{bp}(555)$ and chl*a*. The regression line from Wang et al. (2005) is also shown for comparison. (b) Relationship between modeled $a_t(\lambda)$ and our measured $a_t(\lambda)$ at 412, 443, 490, 510, and 555 nm. Root mean square error (RMSE) at each wavelength is also shown. (c) Relationship between $b_{bp}(555)$ and $a_{NAP}(443)$. High values at stations (stn.) 1, 3, and 207 are circled. For the regression analysis, we excluded the data from station 1 that show extremely high $R_{rs}(\lambda)$ in the green spectral domain (see **Figure 8c**).

Table 5. Mean spectral slopes (±1 SD; N = 183) of CDOM and NAP from this study and the values of $a_{CDOM}(443)$ and $a_{NAP}(443)$.

Mean S_{CDOM}	$a_{CDOM}(443)$	Mean S_{NAP}	$a_{NAP}(443)$
0.0135±0.0027	0.0794	0.0128±0.0012	0.0094

our results show that the performance of chl*a* estimates by the OC4V4 is slightly better than that by the Arctic OC4L (root mean square error (RMSE) of 0.26 and 0.28, respectively). However, when spectra with high $R_{rs}(\lambda)$ in the green spectral domain shown in groups B and C (**Figure 8**) are excluded, the performance of the Arctic OC4L is much better than that of OC4V4 and OC3M (RMSE = 0.13, 0.21, and 0.22, respectively). Since the performance of the ocean color algorithms used here depends on $R_{rs}(\lambda)$ spectral shapes (Equations (5a)–(5c)), the causes of the errors are discussed for each $R_{rs}(\lambda)$ spectral group A–D shown in **Figure 8** that were qualitatively classified in this study as follows: (A) $R_{rs}(\lambda)$ spectra are gradually decreasing toward the blue and red spectral domain with a maximum at 490 nm (red station numbers in **Figure 1**); (B) $R_{rs}(\lambda)$ are high in the green spectral domain, with their values sharply decreasing toward the blue spectral domain (purple station numbers in **Figure 1**); (C) $R_{rs}(\lambda)$ are remarkably high or high and flat in the green spectral domain, with high values in the red spectral domain (yellow station numbers in **Figure 1**); (D) $R_{rs}(\lambda)$ spectral shapes are sharply decreasing toward the red spectral domain, with flat $R_{rs}(\lambda)$ values from 412 to 490 nm (blue station numbers in **Figure 1**). We assume that the performance of the three algorithms does not depend on the solar zenith angle in this study because band-ratio techniques such as MBR strongly reduce its effect (Morel et al., 2002).

For group A, the accuracy of chl*a* estimates by the OC4V4 and OC3M are very similar, and both tend to be underestimated

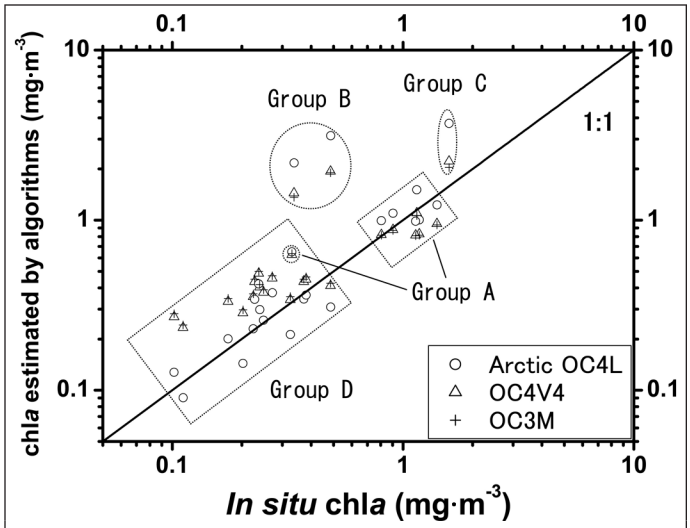

Figure 7. Comparison of chl*a* values estimated by the three algorithms (Arctic OC4L, OC4V4, and OC3M) with measured chl*a* values. The $R_{rs}(\lambda)$ spectral groups A–D correspond to those identified in **Figure 8** and are represented spatially in **Figure 1**. At station 1 in spectral group C, chl*a* was not measured. Station 193 is circled in group D.

except at station 192 (**Figure 7**). The impact on the accuracy of the algorithms due to slight differences in spectral shapes between station 192 and the other stations in this group (**Figure 8a**) is observed. Cota et al. (2004) suggested that chl*a* estimates by the OC4V4 tend to be underestimated at chl*a* > 0.6 mg·m^{-3}, which is consistent with our evaluation in spectral group A. Seawater absorption was dominated by CDOM > 60% in this spectral group, and this effect is clearly shown by decreasing $R_{rs}(\lambda)$ values in the blue spectral domain (**Figure 8a**). On the other hand, the Arctic OC4L performs well (RMSE = 0.13). Geographically, $R_{rs}(\lambda)$ spectral shapes were observed at stations on the Chukchi Sea Shelf and off Point Barrow (red station numbers in **Figure 1**). The spatial distribution is qualitatively consistent with that of warm water (>0 °C) at a salinity (*S*) of 31.5 practical salinity units (psu) (**Figure 9a**), which corresponds to that of Alaskan coastal water (ACW) (Shimada et al., 2001). In groups B and C, the chl*a* is overestimated up to approximately six-fold by the three algorithms (RMSE ranges from 0.11 to 0.81). Because $a_t(\lambda)$ varies little in the green spectral domain and since the variability in the shape of *f*/*Q* is also small (Equation (4a)) (see

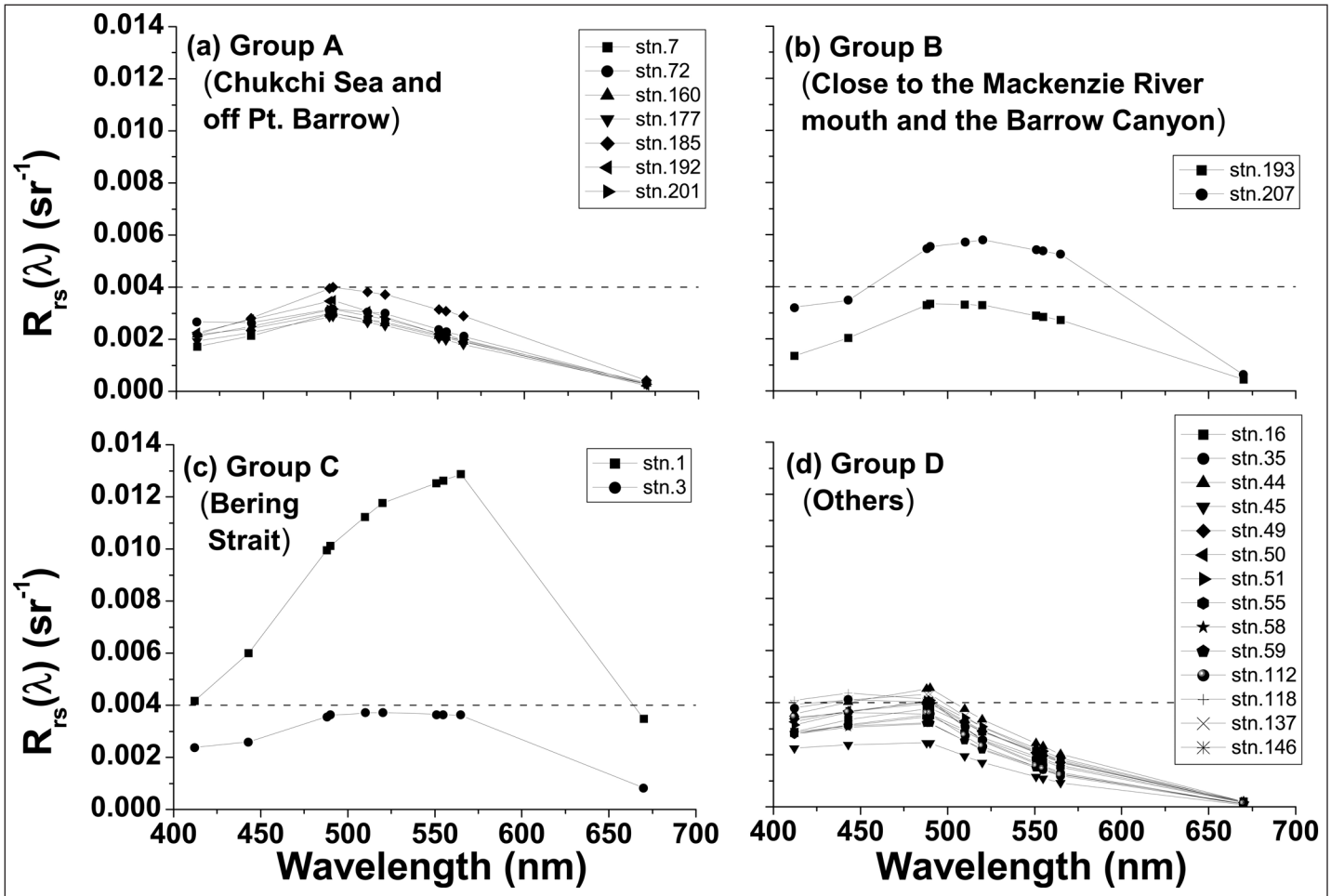

Figure 8. Classified $R_{rs}(\lambda)$ spectral groups A (a), B (b), C (c), and D (d). Locations where $R_{rs}(\lambda)$ values were obtained are indicated in parentheses for each spectral group. Locations for each spectral group are shown as a different color in **Figure 1**. Horizontal lines at the value of 0.004 (sr^{-1}) are drawn to help comparison among the spectral groups.

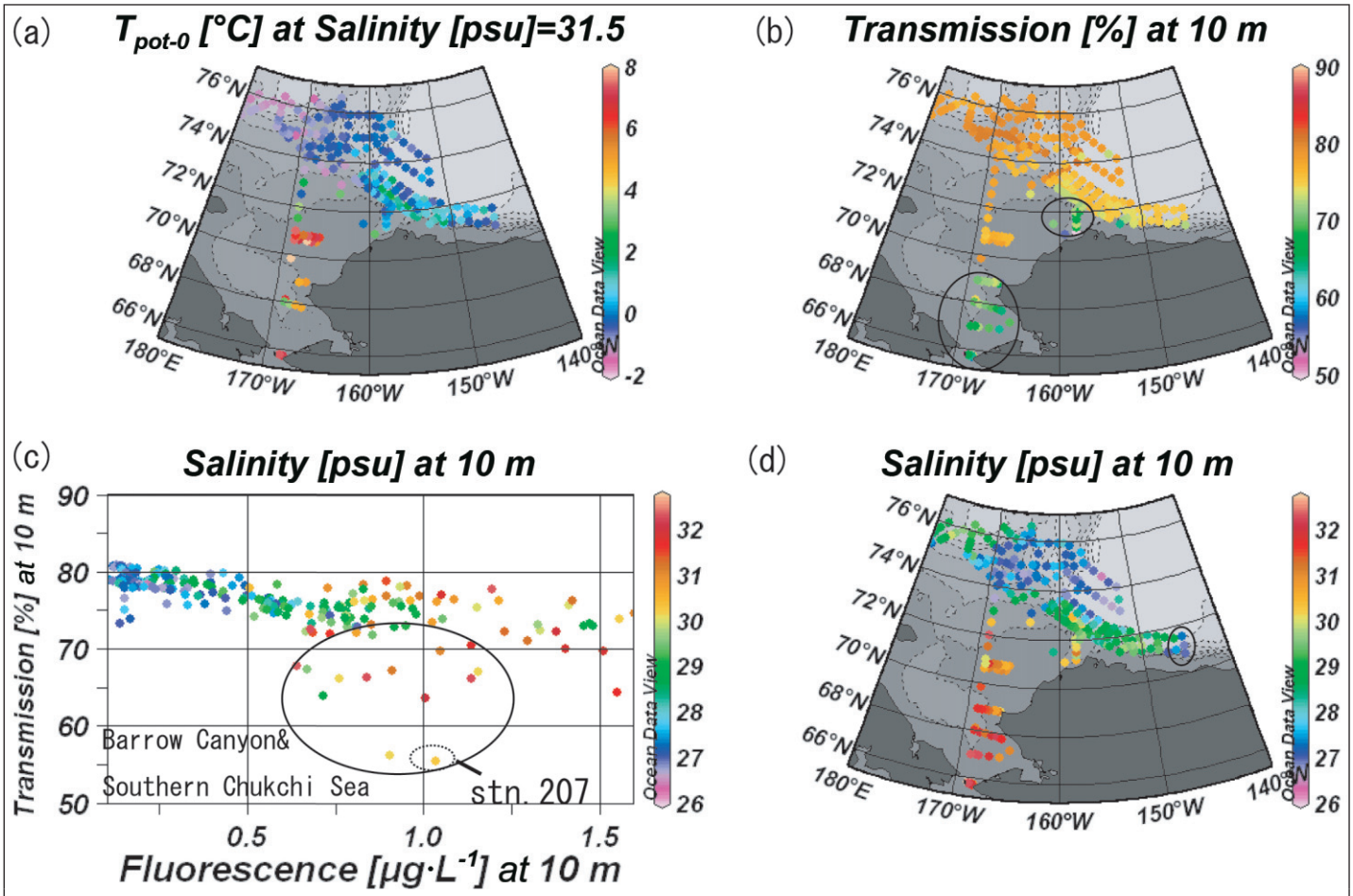

Figure 9. Hydrographic features and their relationship with optical properties. (a) Potential temperature T_{pot} at salinity S = 31.5 psu. The warm temperature (>0 °C) at S = 31.5 psu corresponds to Alaskan coastal water (ACW) (Shimada et al., 2001). (b) Transmission at 10 m depth (representative of surface water). Circles represent the southern Chukchi Sea and the Barrow Canyon where remarkably low transmission was found. (c) Relationship between transmission and fluorescence at 10 m depth. Colors show salinity. Circles represent waters observed in the Barrow Canyon and the southern Chukchi Sea, indicating that the waters contain high concentrations of suspended material. Station 207 located in the Barrow Canyon is circled. (d) Salinity at 10 m depth. The data within the oval represent remarkably low salinity, suggesting that the water originates from the Mackenzie River.

Loisel and Morel, 2001), $b_b(\lambda)$ has a greater impact on higher $R_{rs}(\lambda)$ values in the green spectral domain. During our cruise, we found remarkably turbid waters with a low transmittance in these spectral groups at stations located in the Barrow Canyon and the southern Chukchi Sea (shown as circles in **Figure 9b**). These points are well below the transmission versus fluorescence trend (**Figure 9c**). This is not the case at station 193 (**Figure 9b**) close to the mouth of the Mackenzie River (**Figure 9d**). Although the bio-optical properties are not perfectly correlated with hydrographic features as shown here, our results confirm that the high $b_{bp}(555)$ value (**Figure 6c**) leading the high $R_{rs}(\lambda)$ observed at these stations originates from waters with high suspended matter concentrations. The high $R_{rs}(\lambda)$ in the green spectral domain (**Figures 8b** and **8c**) is the main cause of the errors in chl*a* estimates by the three algorithms in these spectral groups. This leads to lower $R_{rs}(443 > 490 > 510/555)$ values (Equations (5a)–(5c)); at $R_{rs}(443 > 490 > 510/555)$ values less than 1.6, the Arctic OC4L yields higher chl*a* estimates than the OC4V4 (**Figure 10**). Except for groups B and C where waters are turbid, the overestimates of chl*a* by the Arctic OC4L relative to the OC4V4 could be due to a very high packaging effect at $R_{rs}(443 > 490 > 510/555)$ values less than 1.6. Overestimates of chl*a* are thus greater by the Arctic OC4L than by the OC4V4 and OC3M algorithms (**Figure 7**). In group D where $R_{rs}(\lambda)$ was observed offshore (blue station numbers in **Figure 1**), the performance of the Arctic OC4L is good and much better than that of the OC4V4 and OC3M (RMSE = 0.13, 0.23, and 0.24, respectively) (**Figure 7**). The underestimates of chl*a* by the OC4L relative to the OC4V4 at $R_{rs}(443 > 490 > 510/555)$ values greater than 1.6 may be due to the strong CDOM absorption observed in this study (**Figure 10**).

As a result, when groups B and C are excluded, which correspond to waters with high backscattering by particles and show high $R_{rs}(676)$ values (>0.00042 sr^{-1}), the Arctic OC4L performs well (RMSE = 0.13). In other words, the accuracy of

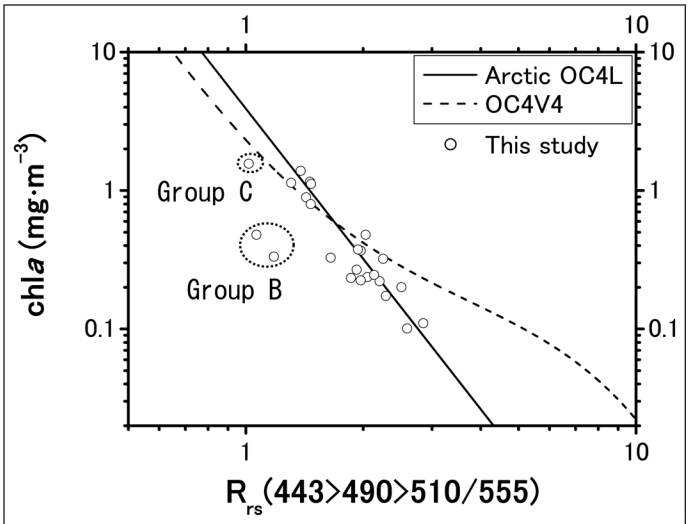

Figure 10. Computed chl*a* using the Arctic OC4L and OC4V4 algorithms with in situ chl*a* as a function of $R_{rs}(443 > 490 > 510/555)$. $R_{rs}(443 > 490 > 510/555)$ represents the maximum band ratio (MBR), namely whichever ratio $R_{rs}(443)/R_{rs}(555)$, $R_{rs}(490)/R_{rs}(555)$, or $R_{rs}(510)/R_{rs}(555)$ is greatest (see the section titled Background: relationship between inherent optical properties (IOPs) and apparent optical properties (AOPs)). Waters classified in $R_{rs}(\lambda)$ spectral groups B and C are circled. Points represent the data obtained in this study.

the Arctic OC4L algorithm is more affected in these $R_{rs}(\lambda)$ spectra than the accuracy of OC4V4 and OC3M. Our analysis shows that no simple empirical algorithm is accurate in these waters. A possible alternative could be the use of semianalytical inversion models (e.g., Carder et al., 1999; Maritorena et al., 2002), which may be more appropriate in these waters. Two other alternatives are also worth investigating because the spectra can easily be classified by a method such as fuzzy classification (Moore et al., 2001) used in tandem with empirical algorithms. Sun-induced chlorophyll fluorescence (e.g., Huot et al., 2007) is also another potentially interesting signal that could be useful in these waters.

Our results, however, raise an interesting conundrum in the waters of the western Arctic Ocean: the absorption of these waters is dominated by strong CDOM (76% at 443 nm), and CDOM does not covary with chl*a* (**Table 2**), but the Arctic OC4L performs well in the western Arctic Ocean. This is only possible if $R_{rs}(443 > 490 > 510/555)$ covaries well with phytoplankton absorption.

Although it is difficult to confirm the impact of $a_{\phi}(\lambda)$ and $a_{CDOM}(\lambda)$ on the $R_{rs}(\lambda)$ ratio without more involved modeling analysis, it is possible to examine this variability using the coefficient of variation (CV), which is equal to the standard deviation divided by the arithmetic mean. The results show that phytoplankton absorption varies approximately 2.4 times as much as CDOM absorption at 443 nm (CV = 0.81 and 0.34 above z_{90}, respectively). This result suggests that while CDOM absorption is relatively constant, phytoplankton absorption varies remarkably. Since NAP absorption contributes the least for the total non-water absorption (**Figure 5**; **Table 4**), the variability of phytoplankton absorption can have a strong impact on chl*a* estimates by ocean color algorithms despite the high CDOM absorption found in this study region. This is compounded by the fact that the CDOM absorption in this region has a particularly low spectral slope compared with those of other oceanic environments (see **Table 5**), which means that its impact on the blue to green ratio is actually approximately two times lower than that of phytoplankton per unit increase in absorption. A rough calculation of their respective impact on the blue to green reflectance ratio can be made by multiplying their coefficient of variation by their fraction of the contribution to total absorption (0.19 and 0.73, respectively, at 490 nm for phytoplankton and CDOM) by the ratio of their absorption spectra at 490 nm to that at 555 nm (4.4 and 2.4, respectively, for phytoplankton and CDOM). This calculation shows that phytoplankton has a roughly equal or slightly larger influence on the blue to green variability despite contributing much less to total absorption. Although the number of data obtained by Cota et al. (2004) from the Arctic Ocean to develop their algorithm is not clear (cited as Cota, unpublished in Cota et al., 2004), it is likely that the larger part of the data used for the Arctic OC4L was obtained from high northern latitudes (cited as Wang and Cota, 2003; Cota et al., 2003; and Cota, unpublished) where CDOM absorption is strong. The reason for the accuracy of the Arctic OC4L algorithm is not well understood, but our analysis suggests that, at least for the western Arctic Ocean, the effect of strong but relatively constant CDOM absorption with a low spectral slope and variability of phytoplankton absorption including a packaging effect seems to underlie this algorithm.

Conclusions

In summary, we found that the light absorption coefficients for both phytoplankton and total particulate fractions as a function of chl*a* are lower in the western Arctic Ocean than in waters at lower latitudes. This can be attributed to larger and (or) more pigmented phytoplankton such as diatoms, which lead to the lower absorption coefficients because of the packaging effect. Although the characteristics of phytoplankton absorptions depart from the norm, the most important feature in these waters is that the total non-water absorption is dominated by strong colored dissolved organic matter (CDOM) absorption, which is significantly higher than that in other environments.

Despite the strong CDOM absorption, our evaluation shows that when turbid waters (remote sensing reflectance $R_{rs}(\lambda) > 0.00042\ sr^{-1}$) are excluded, the Arctic OC4L algorithm performs well relative to OC4V4 and OC3M in our study region. Both strong CDOM absorption and variability of phytoplankton absorption including a package effect seem to be built into the Arctic OC4L, but its performance results from the large effect of phytoplankton absorption on the spectral ratios. This implies that the performance of this algorithm might change when the species composition changes. We also caution

that when waters that show high $R_{rs}(\lambda)$ from the green to red spectral domain are included for chl*a* estimates, the performance of the Arctic OC4L is significantly worse than that of global algorithms. Although we propose a single threshold value for these waters, a better classification scheme based on fuzzy logic (Moore et al., 2001) could prove to apply the Arctic OC4L in the appropriate location. This combination should allow us to accurately estimate chl*a*.

An interesting result meriting further attention is that the spatial distribution of Alaskan coastal water is qualitatively consistent with that of our spectral group. This result implies that some water masses can be separated using these optical properties and observed using ocean color remote sensing. It is thus probable that in this region ocean color sensors may help us understand the dynamic physical features of water masses, which might be related to recent climate change with other available data such as sea surface temperature and sea ice extent (see examples in Platt et al., 2005).

Acknowledgements

We are grateful to the captain and crew of the Japanese R/V *Mirai*, Shigeto Nishino, Sanae Chiba, and Yuichi Sonoyama for their assistance in the collection of data for this study. We also thank H. Kiyofuji, K. Mizobata, and D. Doxaran for their valuable suggestions on this work. Valuable comments by A. Bricaud are much appreciated. This research was funded by the Japan Aerospace Exploration Agency (JAXA) through the program of Arctic research projects using the International Arctic Research Center (IARC) – JAXA Information System (IJIS).

References

Arrigo, K.R., Robinson, D.H., Worthen, D.L., Schieber, B., and Lizotte, M.P. 1998. Bio-optical properties of the southern Ross Sea. *Journal of Geophysical Research*, Vol. 103, No. C10, pp. 21 683 – 21 695.

Babin, M., Stramski, D., Ferrari, G. M., Claustre, H., Bricaud, A., Obolensky, G., and Hoepffner, N. 2003. Variations in the light absorption coefficients of phytoplankton, nonalgal particles, and dissolved organic matter in coastal waters around Europe. *Journal of Geophysical Research*, Vol. 108, No. C7, 3211, doi:10.1029/2001JC00082.

Bricaud, A., Babin, M., Morel, A., and Claustre, H. 1995. Variability in the chlorophyll-specific absorption coefficients of natural phytoplankton: analysis and parameterization. *Journal of Geophysical Research*, Vol. 100, No. C7, pp. 13 321 – 13 332.

Bricaud, A., Morel, A., Babin, M., Allaili, K., and Claustre, H. 1998. Variations of light absorption by suspended particles with chlorophyll a concentration in oceanic (case 1) waters: analysis and implications for bio-optical models. *Journal of Geophysical Research*, Vol. 103, No. C13, pp. 31 033 – 31 044.

Carder, K.L., Steward, R.G., Harvey, G.R., and Ortner, P.B. 1989. Marine humic and fulvic acids: their effects on remote sensing of ocean chlorophyll. *Limnology and Oceanography*, Vol. 34, No. 1, pp. 68–81.

Carder, K.L., Chen, F.R., Lee, Z.P., Hawes, S.K., and Kamykowski, D. 1999. Semianalytic moderate-resolution imaging spectrometer algorithms for chlorophyll a and absorption with bio-optical domains based on nitrate-depletion temperatures. *Journal of Geophysical Research*, Vol. 104, No. C3, pp. 5403–5421.

Chen, M., Yipu, H., Laodong, G., Pingphe, C., Weifeng, Y., Guangshan, L., and Yusheng, Q. 2002. Biological productivity and carbon cycling in the Arctic Ocean. *Chinese Science Bulletin*, Vol. 47, No. 12, pp. 1037–1040.

Cleveland, J.S., and Weidemann, A.D. 1993. Quantifying absorption by aquatic particles: a multiple scattering correction for glass-fiber filters. *Limnology and Oceanography*, Vol. 38, No. 6, pp. 1321–1327.

Cota, G.F., Harrison, W.G., Platt, T., Sathyendranath, S., and Stuart, V. 2003. Bio-optical properties of the Labrador Sea. *Journal of Geophysical Research*, Vol. 108, No. C7, 3228, doi:10.1029/2000JC000597.

Cota, G.F., Wang, J., and Comiso, J.C. 2004. Transformation of global satellite chlorophyll retrievals with a regionally tuned algorithm. *Remote Sensing of Environment*, Vol. 90, pp. 373–377.

Darecki, M., and Stramski, D. 2004. An evaluation of MODIS and SeaWiFS bio-optical algorithms in the Baltic Sea. *Remote Sensing of Environment*, Vol. 89, No. 3, pp. 326–350.

Dierssen, H.M., and Smith, R.C. 2000. Bio-optical properties and remote sensing ocean color algorithms for Antarctic Peninsula waters. *Journal of Geophysical Research*, Vol. 105, No. C11, pp. 26 301 – 26 312.

Esaias, W.E., Abott, M.R., Barton, I., Brown, O.B., Campbell, J.W., Carder, K.L., Clark, D.K., Evans, R.H., Hoge, F.E., Gordon, H.R., Balch, W.M., Letelier, R., and Minnett, P.J. 1998. An overview of MODIS capabilities for ocean science observation. *IEEE Transactions on Geoscience and Remote Sensing*, Vol. 36, No. 4, pp. 1250–1265.

Gordon, H.R., and McCluney, W.R. 1975. Estimation of the depth of sunlight penetration in the sea for remote sensing. *Applied Optics*, Vol. 14, No. 2, pp. 413–416.

Holm-Hansen, O., Lorenzen, C.J., Holmes, R.W., and Strickland, J.D.H. 1965. Fluorometric determination of chlorophyll. *Journal du Conseil, Conseil International pour l'Exploration de la Mer*, Vol. 30, No. 1, pp. 3–15.

Huot, Y., Brown, C.A., and Cullen, J.J. 2007. Retrieval of phytoplankton biomass from simultaneous inversion of reflectance, the diffuse attenuation coefficient, and Sun-induced fluorescence in coastal waters. *Journal of Geophysical Research*, Vol. 112, No. C06013, doi:10.1029/2006JC003794.

Kirk, J.T.O. 1994. *Light and photosynthesis in aquatic ecosystems*. Cambridge University Press, New York.

Kishino, M., Takahashi, M., Okami, N., and Ishimaru, S. 1985. Estimation of the spectral absorption coefficients of phytoplankton the sea. *Bulletin of Marine Science*, Vol. 37, No. 2, pp. 634–642.

Lee, Z.P., Carder, K.L., and Arnone, R.A. 2002. Deriving inherent optical properties from water color: a multiband quasi-analytical algoritm for optically deep waters. *Applied Optics*, Vol. 41, No. 27, pp. 5755–5772.

Lee, Z.P., Du, K.-P., and Arnone, R. 2005. A model for diffuse attenuation coefficient of downwelling irradiance. *Journal of Geophysical Res*earch, Vol. 110, No. C2, C02016, doi:10.1029/2004JC002275.

Loisel, H., and Morel, A. 2001. Non-isotropy of the upward radiance field in typical coastal (Case 2) waters. *International Journal of Remote Sensing*, Vol. 22, No. 2, pp. 275–295.

Maritorena, S., Siegel, D.A., and Peterson, A.R. 2002. Optimization of a semianalytical ocean color model for global-scale applications. *Applied Optics*, Vol. 41, No. 15, pp. 2705–2713.

Marrari, M., Hu, C., and Daly, K. 2006. Validation of SeaWiFS chlorophyll a concentrations in the Southern Ocean: a revisit. *Remote Sensing of Environment*, Vol. 105, pp. 367–375.

Mitchell, B.G. 1990. Algorithms for determining the absorption coefficient for aquatic particles using the quantitative filter technique. In *Ocean Optics X,* 16–18 April 1990, Orlando, Fla. Edited by R.W. Spinrad. Proceedings of SPIE Volume 1302, The International Society for Optical Engineering (SPIE), Bellingham, Wash. pp. 137–148.

Mitchell, B.G. 1992. Predictive bio-optical relationships for polar oceans and marginal ice zones. *Journal of Marine Systems*, Vol. 3, pp. 91–105.

Mitchell, B.G., and Holm-Hansen, O. 1991. Bio-optical properties of Antarctic Peninsula waters: differentiation from temperate ocean models. *Deep-Sea Research*, Vol. 38, No. 8–9A, pp. 1009–1028.

Moore, T.S., Campbell, J.W., and Feng, H. 2001. A fuzzy logic classification scheme for selecting and blending satellite ocean color algorithms. *IEEE Transactions on Geoscience and Remote Sensing*, Vol. 39, No. 8, pp. 1764–1776.

Morel, A. 1974. Optical properties of pure water and pure seawater. In *Optical aspects of oceanography*. Edited by N.G. Jerlov and E. Steemann Nielson. Academic Press, London. pp. 1–24.

Morel, A., and Bricaud, A. 1981. Theoretical results concerning light absorption in a discrete medium, and application to specific absorption of phytoplankton. *Deep-Sea Research*, Vol. 28A, No. 11, pp. 1375–1393.

Morel, A., and Maritorena, S. 2001. Bio-optical properties of oceanic waters: a reappraisal. *Journal of Geophysical Research*, Vol. 106, No. C4, pp. 7163–7180.

Morel, A., Antoine, D., and Gentili, B. 2002. Bidirectional reflectance of oceanic waters: accounting for Raman emission and varying particles phase function. *Applied Optics*, Vol. 41, No. 30, pp. 6289–6306.

Muller, J.L., and Austin, R.W. 1995. *Ocean optics protocols for SeaWiFS validation, Revision 1*. National Aeronautics and Space Administration (NASA), Greenbelt, Md. NASA Technical Memorandum 104566, Vol. 25.

O'Reilly, J.E., Maritorena, S., Mitchell, B.G., Siegel, D.A., Carder, K.L., Garver, S.A., Kahru, M., and McClain, C. 1998. Ocean color chlorophyll algorithms for SeaWiFS. *Journal of Geophysical Research*, Vol. 103, No. C11, pp. 24 937 – 24 953.

O'Reilly, J.E., Maritorena, S., O'Brien, M.C., Siegel, D.A., Toole, D., Menzies, D., Smith, R.C., Mueller, J.L., Mitchell, B.G., Kahru, M., Chavez, F.P., Strutton, P., Cota, G.F., Hooker, S.B., McClain, C.R., Carder, K.L., Muller-Karger, F., Harding, L., Magnuson, A., Phinney, D., Moore, G.F., Aiken, J., Arrigo, K.R., Letelier, R., and Culver, M. 2000. *SeaWiFS postlaunch calibration and validation analyses, part 3*. National Aeronautics and Space Administration (NASA), Greenbelt, Md. NASA Technical Memorandum 2000-206892, Vol. 11.

Platt, T., Bouman, H., Devred, E., Fuentes-Yaco, C., and Sathyendranath, S. 2005. Physical forcing and phytoplankton distributions. *Science Marina*, Vol. 69, pp. 55–73.

Pope, R.M., and Fry, E.S. 1997. Absorption spectrum (380–700 nm) of pure water. 2. Integrating cavity measurements. *Applied Optics*, Vol. 36, No. 33, pp. 8710–8723.

Sathyendranath, S., Cota, G., Stuart, V., Maass, H., and Platt, T. 2001. Remote sensing of phytoplankton pigments: a comparison of empirical and theoretical approaches. *International Journal of Remote Sensing*, Vol. 22, No. 2–3, pp. 249–273.

Shiklomanov, I.A. 1993. World fresh water resources. In *Water in crisis: a guide to the world's fresh water resources*. Edited by P.H. Gleick. Oxford University Press, New York. pp. 13–24.

Shimada, K., Carmack, E.C., Hatakeyama, K., and Takizawa, T. 2001. Varieties of shallow temperature maximum waters in the western Canadian basin of the Arctic Ocean. *Geophysical Research Letters*, Vol. 28, No. 18, pp. 3441–3444.

Springer, A.M., McRoy, C.P., and Frinnt, M.V. 1996. The Bering Sea green belt: shelf-edge processes and ecosystem production. *Fisheries Oceangraphy*, Vol. 5, No. 3–4, pp. 205–223.

Stramska, M., Stramski, D., Hapter, R., Kaczmarek, S., and Ston, J. 2003. Bio-optical relationships and ocean color algorithms for the north polar region of the Atlantic. *Journal of Geophysical Research*, Vol. 108, No. C5, 3143, doi:10.1029/2001JC001195.

Stramski, D., Boss, E., Bogucki, D., and Boss, K.J. 2004. The role of seawater constituents in light backscattering in the ocean. *Progress in Oceanography*, Vol. 61, pp. 27–56.

Suzuki, R., and Ishimaru, T. 1990. An improved method for the determination of phytoplankton chlorophyll using n,n-dimethylformamide. *Journal of Oceanography*, Vol. 46, pp. 190–194.

Wang, J., and Cota, G.F. 2003. Remote-sensing reflectance in the Beaufort and Chukchi seas: observations and models. *Applied Optics*, Vol. 42, No. 15, pp. 2754–2765.

Wang, J., Cota, G.F., and Ruble, D.A. 2005. Absorption and backscattering in the Beaufort and Chukchi seas. *Journal of Geophysical Research*, Vol. 110, No. C04014, doi:10.1029/2002JC001653.

List of symbols

$a_t(\lambda)$, $a_{t\text{-}w}(\lambda)$, $a_\varphi(\lambda)$, $a_{NAP}(\lambda)$, $a_p(\lambda)$, $a_{CDOM}(\lambda)$, $a_w(\lambda)$	total, total non-water, phytoplankton, NAP, total particulate fractions (phytoplankton plus NAP), CDOM, and pure seawater absorption coefficients at λ (m^{-1})
$a_\varphi^*(\lambda)$	chlorophyll-*a*-specific absorption coefficient of phytoplankton at λ ($m^2 \cdot mg\ chl a^{-1}$)
$A_x(\lambda)$, $E_x(\lambda)$	empirically derived coefficients for power law $a_x(\lambda) = A_x(\lambda)[chl a]^{E_x(\lambda)}$, where x can be p, φ, NAP, CDOM, and t (dimensionless)
$b_{bp}(\lambda)$, $b_{bw}(\lambda)$, $b_b(\lambda)$	particle, pure seawater, and total backscattering coefficients at λ (m^{-1})
chl(OC4L), chl(OC4V4), chl(OC3M)	estimated chl*a* by the Arctic OC4L, OC4V4, and OC3M ocean color algorithms ($mg \cdot m^{-3}$)
$E_d(\lambda, z)$	downwelling irradiance at λ at z ($\mu W \cdot cm^{-2} \cdot nm^{-1}$)

$K_d(\lambda)$	diffuse attenuation coefficient of downwelling irradiance at λ (m^{-1})
$L_u(\lambda, z)$, $L_w(\lambda, z)$	upwelling radiance and water-leaving radiance at λ at z ($\mu W \cdot cm^{-2} \cdot nm^{-1} \cdot sr^{-1}$)
$L_{wn}(\lambda)$	normalized water-leaving radiance at λ ($\mu W \cdot cm^{-2} \cdot nm^{-1} \cdot sr^{-1}$)
$OD_p(\lambda)$, $OD_{NAP}(\lambda)$	optical density of total particulate fractions (phytoplankton plus NAP) and NAP at λ (dimensionless)
$R_{rs}(\lambda)$	remote sensing reflectance at λ (sr^{-1})
z, z_{90}, z_e	geometric depth, first optical depth (90% of the upwelling radiance originates), and euphotic depth (1% of surface light level) (m)
λ	wavelength (nm)